Interface Properties of CoPc on Nanographene Covered Au(111) and the Influence of Annealing

Axel Belser,[†] Katharina Greulich,[†] Marie S. Sättele,[†#] Michael Fingerle,[#] Ruslan Ovsyannikov,[§] Erika Giangrisostomi,[§] Thomas Chassé,[†‡] and Heiko Peisert[†]*

† Institute of Physical and Theoretical Chemistry, University of Tübingen, Auf der Morgenstelle 18, 72076 Tübingen, Germany

Institute of Organic Chemistry, University of Tübingen, Auf der Morgenstelle 18, 72076 Tübingen, Germany

§ Institute for Methods and Instrumentation in Synchrotron Radiation Research, Helmholtz-Zentrum Berlin für Materialien und Energie GmbH, Albert-Einstein-Straße 15, 12489 Berlin, Germany

‡ Center for Light-Matter Interaction, Sensors & Analytics (LISA[+]) at the University of Tübingen, Auf der Morgenstelle 18, 72076 Tübingen, Germany

* Corresponding author, heiko.peisert@uni-tuebingen.de, Tel.: (+49) 07071 / 29-76931, Fax: (+49) 07071 / 29-5490

Abstract

Organic bilayer systems and heterostructures are of enormous importance for optoelectronic devices. We study interface properties and the structural ordering of cobalt phthalocyanine (CoPc) on a highly ordered monolayer (ML) hexa-*peri*-hexabenzocoronene (HBC), grown on Au(111), using photoemission, X-ray absorption (XAS), scanning tunneling microscopy (STM) and low-energy electron diffraction (LEED). A charge transfer between CoPc and the gold substrate is almost completely prevented by the HBC intermediate layer. We show that HBC acts as a template for the initial growth of CoPc molecules. After annealing to 630 K, a molecular exchange takes place, resulting in a coexistence of domains of both CoPc and HBC molecules at the surface.

Keywords hexa-*peri*-hexabenzocoronene, cobalt phthalocyanine, transition metal phthalocyanines, bilayers, intermediate layer, valence band, π-conjugated systems, orientation, interaction, photoemission, x-ray absorption spectroscopy, near edge x-ray absorption fine structure, scanning tunneling microscopy, low-energy electron diffraction

1. Introduction

The tuning of electronic interface properties between organic molecules and metallic substrates is of enormous importance for a broad variety of applications.[1-7] Strong interactions including chemical reactions may alter the molecular electronic structure of the frontier orbitals, which are important for charge carrier transport and injection. Routes to avoid chemical interactions at interfaces include, among others, the optimization of the surface preparation or the introduction of intermediate layers.[8-13] Such intermediate layers can be of different nature, a well-known representative is the 2D material graphene. However, the number of substrates enabling growth of well-defined graphene layers is limited. Best growth conditions are achieved for perfect (111) single crystal surfaces with reasonable lattice matching.[14-15] Although even on Au(111) a direct growth of graphene can only be reached at comparably high temperatures, the formation of graphene islands cannot be excluded.[16-17]

An alternative route to establish an intermediate carbon layer on Au(111) under gentle preparation conditions could be the preparation of a well-ordered monolayer of nanographene molecules. The possibly best-known representative of nanographene molecules is hexa-*peri*-hexabenzocoronene (HBC), a planar polycyclic aromatic hydrocarbon (PAH) with noble electronic properties.[18-19] Well-ordered HBC monolayers with large domains can be easily prepared by deposition of several layers and subsequent annealing.[20-23] The stability of molecular intermediate layers will essentially depend on the strength of the molecule-substrate interaction. If the molecule-substrate interaction for molecules deposited subsequently on the intermediate layer is significantly stronger than for molecules of the first (intermediate) layer, a molecular

exchange can take place.[24-29] For the PTCDA/CuPc/Ag(111) such effects were already observed at very low temperatures (1.1 K).[28] In contrast, pentacene/para-sexiphenyl/Cu(111) is stable against molecular exchange at 15 K and only after annealing to 300 K an irreversible reversed bilayer is formed.[26] Thus, molecular exchange depends crucially on the combination of the materials, which has been investigated for several bilayer model systems.[21, 26-28, 30-33]

In the present study we address the question if an HBC intermediate layer on Au(111) is stable against molecular exchange with phthalocyanine molecules. Cobalt phthalocyanine (CoPc) was chosen as a representative for the family of phthalocyanines, because of its well-known interaction with the gold substrate (interfacial charge transfer).[34-35] The stability was monitored up to temperatures of 630 K, which may simulate a long-term stability. The experimental procedure is illustrated in **Figure 1**.

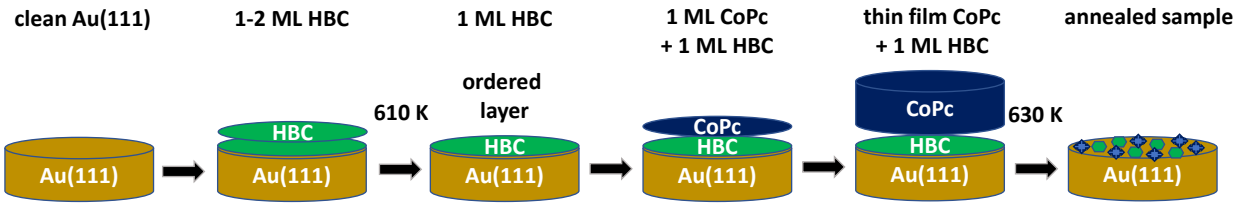

Figure 1. *Experimental procedure. First, 2-3 monolayers of HBC were deposited on a well-defined Au(111) surface and subsequently annealed to 610 K to form a homogeneous monolayer. On top, CoPc was deposited in a stepwise manner. Finally, the sample was annealed to 630 K.*

2. Experimental Section

The Au(111) single crystal was cleaned by repeated cycles of each 30 min Ar^+-ion sputtering at a voltage of 0.8 kV and a partial pressure of $5 \cdot 10^{-5}$ mbar and subsequent annealing to 770 K. The purity and orientation of the crystal was checked by x-ray photoelectron spectroscopy (XPS), ultraviolet photoelectron spectroscopy (UPS), scanning tunneling microscopy (STM) and low-energy electron diffraction (LEED). HBC was synthesized as described previously.[36] CoPc was purchased from Sigma-Aldrich. The molecules were evaporated from a Knudsen cell at rates of 0.2 - 0.5 nm/min, controlled by a quartz crystal microbalance (QCM). The nominal layer thickness was estimated from substrate and adsorbate related XPS intensity ratios using photoemission cross sections from Yeh and Lindau;[37] the mean free path of photoelectrons was estimated according to Seah and Dench.[38] To produce a closed, highly ordered monolayer, 2-3 layers of HBC were evaporated on the Au(111) single crystal, followed by an annealing of the sample to 610 K for about 15 min. During all deposition steps the crystal was held at room temperature at a pressure of $< 3 \cdot 10^{-8}$ mbar.

All experiments were performed in UHV systems with a base pressure of $2 \cdot 10^{-10}$ mbar. The STM and LEED measurements were carried out in a two-chamber system equipped with a variable temperature (VT)-STM from Omicron GmbH and a LEED optics from OCI Vacuum Microengineering Inc. For the STM measurements, mechanically cut Pt/Ir tips were used. Tip and sample were held at room temperature. Tunneling voltages refer to the tip with respect to the sample. The program WSxM was used to improve the contrast of the shown STM images.[39]

The photoelectron spectroscopy (PES) measurements of the core-levels were performed using a multi-chamber UHV system equipped with a Phoibos 150 hemispherical energy analyzer (SPECS), and an X-ray source (Al-K_α radiation, hν = 1486.7 eV) with monochromator (XR 50 M, SPECS). The energy scale was calibrated reproducing the binding energies (BE) of Cu $2p_{3/2}$ and Au $4f_{7/2}$ at 932.56 eV and 84.00 eV, respectively. The peak fitting of core level spectra was performed using Unifit version 2018.[40] A Voigt profile (convolution of Lorentzian and Gaussian profiles) and a Shirley model background was used. The error of absolute binding energies is estimated to be less than ± 0.05 eV.

The X-ray absorption spectroscopy (XAS) and PES measurements of the valence band have been performed using synchrotron radiation at the LowDose-PES endstation of the PM4 beamline at BESSY II (Helmholtz-Zentrum, Berlin, Germany).[41-42] The endstation is equipped with an angle-resolved time-of-flight (ArTOF) analyzer, which was used for PES measurements by integrating over an angle range of ±15°. The improved detection efficiency by a factor of 2-3 orders of magnitude with respect to conventional hemispherical analyzers,[41] allows the study of sensitive organic molecules with limited photon flux. For valence band spectra the energy resolution was about 40 meV (hν = 40.8 eV), 55 meV (hν = 75 eV) and 120 meV (hν = 110 eV). The energy resolution of XAS was about 100 meV and 250 meV at a photon energy (hν) of 400 and 780 eV, respectively. The absorption was monitored indirectly in total electron yield (TEY) mode by measuring the sample current.

3. Results and Discussion

3.1. CoPc Growth on HBC/Au(111) from Monolayer to Thin Films

The structural ordering of the first monolayer may affect the structure and ordering of subsequent layers in many cases (e.g. refs. [43-45]). Therefore, we will first discuss the arrangement of HBC molecules forming the intermediate (mono-)layer on Au(111).

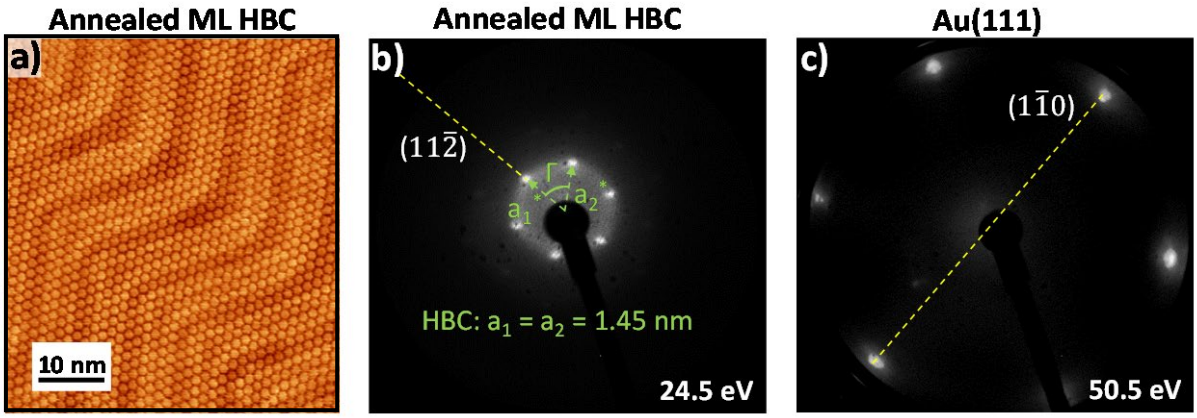

Figure 2. *a) STM image of the intermediate HBC ML (U = 1.3 V, I = 800 pA), b) LEED pattern of the intermediate HBC ML at 24.5 eV, c) LEED pattern of the Au(111) substrate at 50.5 eV for comparison.*

In **Figure 2** STM and LEED images of the HBC monolayer (ML) are shown, prepared by deposition of a multilayer and subsequent annealing to 610 K for 15 minutes. In the STM image of **Figure 2a**, the HBC molecules and the long-range herringbone reconstruction of the underlying Au(111) substrate are clearly visible. The molecules are aligned along the herringbone structure ((11$\bar{2}$)-directions) of the substrate, forming a highly ordered layer. The corresponding LEED pattern at 24.5 eV shows very bright spots in the Au-(11$\bar{2}$) directions (**Figure 2b**). The comparison to

reference pattern from the bare Au(111) substrate taken at 50.5 eV (**Figure 2c**) allows the construction of the HBC unit cell. Since substrate related spots are visible in the $(1\bar{1}0)$ direction, we can deduce that the HBC lattice is rotated by 30° with respect to the unreconstructed Au(111) surface, as reported in other studies.[20-21, 46] The determined lattice parameters obtained from STM and LEED ($a_1 = a_2 = 1.45$ nm, angle between the lattice vectors of $\Gamma = 60°$) are in good agreement to the literature.[20, 46] From their more detailed studies, those authors conclude a commensurate $(\sqrt{27}x\sqrt{27})$R30°-superstructure for the HBC monolayer on Au(111).

In order to evaluate the stability of the highly ordered HBC monolayer on Au(111), about 0.8 - 0.9 ML of CoPc were subsequently deposited on top. New structures are clearly visible in the STM images of **Figure 3**. Large scale STM images are shown as supporting information (**Figure S1**). Some CoPc molecules agglomerate in islands, visible as bright areas in **Figure 3a**, resulting in an apparently lower quality of the image. But nevertheless, three different directions of CoPc rows, which are rotated by 60° to each other can be identified, indicated by blue arrows in **Figure 3a**. A zoom into one of the domains (**Figure 3b**) reveals more details: In broader rows mostly three CoPc molecules are arranged side by side. These rows are aligned at the herringbone of the Au(111) substrate, similar to the HBC molecules of the annealed monolayer (**Figure 2**). In between these broader rows, rows of single molecules can be identified. A line profile was generated along the blue line in **Figure 3b**, depicted in **Figure 3d.** The average apparent height of the rows is about 0.2 nm, indicating the presence of single, flat lying CoPc molecules. Apparent heights in this range were reported for single CoPc molecules on various substrate surfaces (e.g. Ref.[47]; cf. also **Figure 3e**).

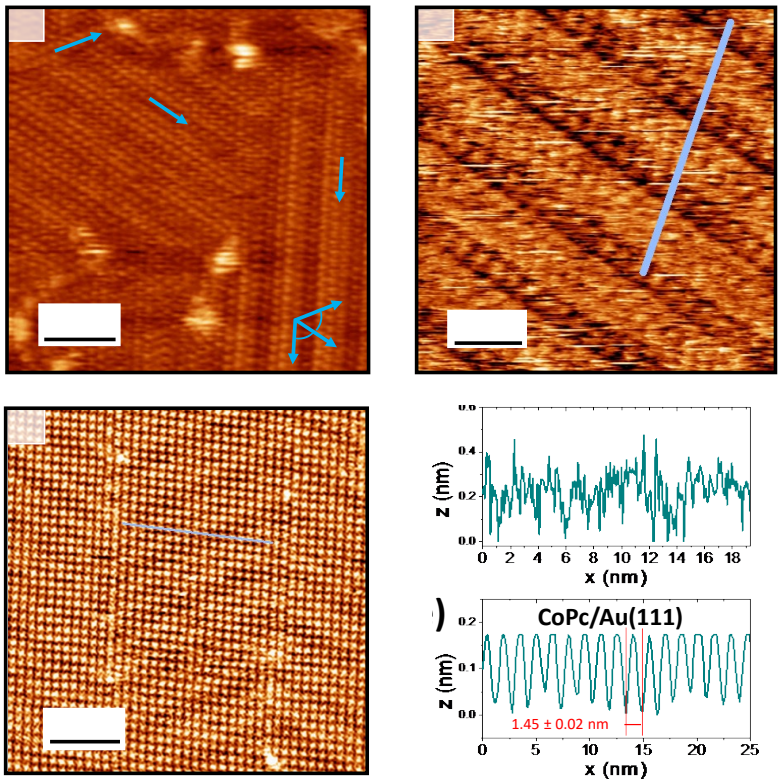

Figure 3. *STM images of 0.8 - 0.9 ML of CoPc deposited on HBC/Au(111) and directly on Au(111) and the respective line profiles: a) About a ML of CoPc on HBC/Au(111) on the domain boundaries (U = 1.6 V, I = 700 pA), b) Zoom in a CoPc domain on HBC/Au(111) (U = 1.3 V, I = 500 pA), c) annealed ML of CoPc on Au(111) (U = 1.2 V, I = 500 pA), d) respective line profile of CoPc on HBC/Au(111), e) respective line profile of CoPc on Au(111).*

We note that similar rows were also observed for sub-monolayer coverages of CoPc on Au(111),[48] and other metal-phthalocyanines on HOPG and Ag(111).[49-50] However, the CoPc rows on HBC/Au(111) appear more uniform compared to the rows formed on other substrates. The threefold symmetry suggests a templating effect of the substrate and/or the well-ordered HBC monolayer. Thus, a reason for the ordered growth might be an optimization of the CoPc-substrate and CoPc-CoPc interaction strength, i.e. the mobility of the CoPc molecules is high

enough for the diffusion to energetically favored adsorption places (due to comparably weak CoPc-substate interactions), whereas at the same time the templating effect by the substrate is still present. Further, at a coverage of exactly one monolayer, as prepared in this experiment, the formation of highly ordered molecular structures might be stabilized.[48] Further, it is known that the substrate roughness and cleanliness may affect distinctly the arrangement order of organic films on gold.[51] We note that data of electronic interface properties indicate that there is no noticeable molecular exchange between HBC molecules of the first monolayer and CoPc (see below). Thus, the presence of HBC molecules in the top layer appears unlikely.

For comparison, 1-2 monolayers of CoPc were deposited directly on Au(111) and heated subsequently to 610 K to form a ML without defects. In contrast to CoPc on HBC/Au(111), the STM image of **Figure 3c** reveals a long-range square ordering of the CoPc molecules. A square adsorption geometry of CoPc and other TMPcs was reported on various substrate surfaces including Au(111).[52-58] From **Figure 3c** a line profile (blue line) was generated, shown in **Figure 3e.** The line profile illustrates the high regularity of the formed CoPc ML and allows an accurate determination of the lattice parameters: $a_1 = a_2 = 1.45 \pm 0.02$ nm. This value is in good agreement with recently published lattice parameters of quadratic ordered monolayers of CoPc and other transition metal phthalocyanines (TMPcs).[52, 55, 59-60] Three different domains aligned to the direction of the herringbone reconstruction of the Au(111) substrate can be observed (see below). The presence of such different domains of CoPc and CuPc on Au(111) was investigated in detail in previous studies.[48, 60-62]

In order to average over larger sample areas, we show in **Figure 4** LEED patterns corresponding to **Figure 3**. In the LEED image of the 0.8 - 0.9 ML CoPc layer on HBC/Au(111) taken at 18.5 eV

(**Figure 4a**), patterns of both the CoPc overlayer and the HBC/Au(111) substrate can be identified, marked by red and green arrows, respectively. The CoPc spots form a hexagonal pattern inside the hexagonal pattern of the HBC molecules and thus the lattice parameters obtained from LEED are larger, we obtain $a_1 = a_2 = 1.78 \pm 0.02$ nm. The angle between the lattice vectors is the same as for the annealed HBC monolayer ($\Gamma = 60°$).

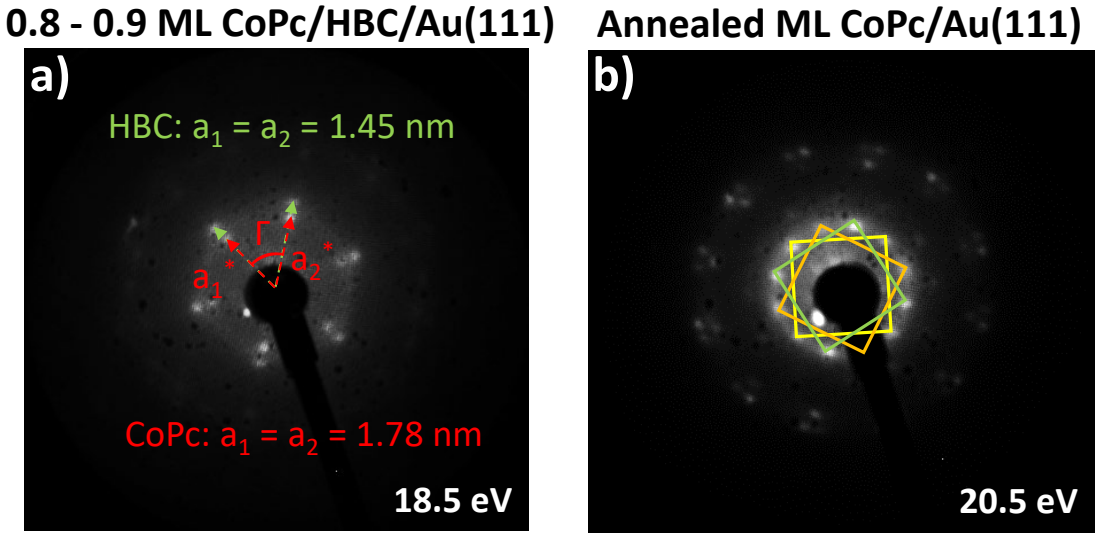

Figure 4. *LEED pattern of CoPc monolayers: a) about a ML CoPc on HBC/Au(111) at 18.5 eV, b) an annealed ML CoPc on Au(111) at 20.5 eV.*

The determination of the lattice parameters for CoPc deposited directly on Au(111) by LEED (**Figure 4b**) is less precise than a determination by STM due to the missing substrate-related spots at this energy. However, the LEED pattern in **Figure 4b** confirms the presence of three different domains, observed already in several STM images. The pattern of the "inner ring" can be interpreted as a superposition of three square patterns rotated by 120˚ (green, orange and yellow

squares in **Figure 4b**) and outer pattern consists of 12x3 spots, as previously reported and discussed in detail for CuPc on Au(111) and MoS_2.[62-63] LEED spots corresponding to different domains do not exhibit the same intensity in **Figure 4b**, which indicates that the three domains are not equally distributed in the probed area.

Remarkably, the lattice parameters of the hexagonal unit cell for CoPc/HBC/Au(111) are distinctly larger compared to the square unit cell (CoPc/Au(111)), i.e. the CoPc molecules are more densely packed on Au(111). The area per molecule is 4.75 nm^2 and 4.2 nm^2 for CoPc on HBC/Au(111) and Au(111), respectively. The different geometry of the unit cell and the different packing density illustrates nicely the templating effect of the Au(111) substrate, which can be tuned by the introduction of intermediate layers.

To gain further information about the molecular orientation of CoPc on HBC/Au(111) as a function of the film thickness, polarization dependent X-ray absorption spectra at the N-K edge were taken for CoPc/HBC/Au(111). N1s π*-excitations can be used in a similar manner as C1s π*-excitations for the analysis of the molecular orientation of TMPcs.[44, 64-67] For CoPc on HBC, C1s π*-excitations are in superposition with HBC related transitions and cannot be used for the determination of the orientation. In **Figure 5**, polarization dependent N-K edge spectra for a 0.3 nm CoPc layer (about 1 ML) and a thin film of 1.5 nm thickness are shown for the two prominent angles corresponding to grazing (θ = 10°) and normal (θ = 90°) incidence of the incoming p-polarized synchrotron light. The measurement geometry is shown as an inset in **Figure 5**. We can essentially distinguish between two regions: Features at photon energies < 402 eV arise predominantly from transitions into π*-orbitals, while feature at higher energies are attributed to transitions into σ*-orbitals. Both XAS for the 0.3 and the 1.5 nm thick layers show essentially

the same dichroism: The maximal intensity for π*-transitions is visible at grazing incidence, while for normal incidence maximal intensity is obtained from σ*-transitions. This indicates a flat lying adsorption geometry in both cases. Remaining intensity in the π*-region of normal incidence spectra is hardly detectable, indicating very small tilt angles (< 10°). The result is in good agreement to CoPc multilayer films on related substrates, such as graphene/Au/Ni(111) and CoPc/Au(111).[8, 58]

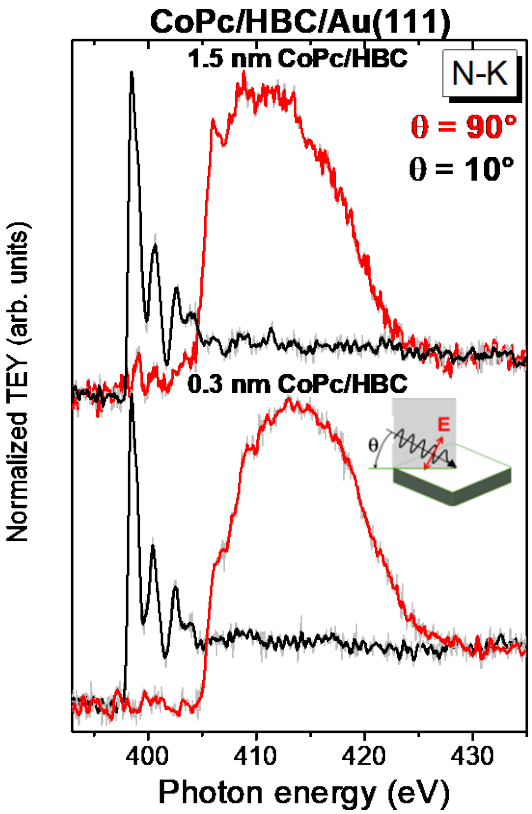

Figure 5. *N-K X-ray absorption spectra of CoPc on a ML of HBC on Au(111) for two different CoPc thicknesses. The red curves correspond to an angle of incidence of 90° (normal incidence) and the black curves to 10° (grazing incidence). The measurement geometry is shown as an inset. The preferred flat lying adsorption geometry is maintained essentially in thicker films of 1.5 nm.*

3.2. Electronic Interface Properties of CoPc on HBC/Au(111)

For CoPc on Au clear interactions between the molecules and the metal substrate were observed, including a charge transfer to the central Co ion (e.g. Refs.[34-35, 68]). Charge transfer cannot always be completely prevented by an intermediate layer, as reported for CoPc on graphene/Ni(111).[34] Therefore the question arises whether the HBC intermediate layer on Au(111) provokes an electronic decoupling of CoPc molecules from the Au(111) substrate.

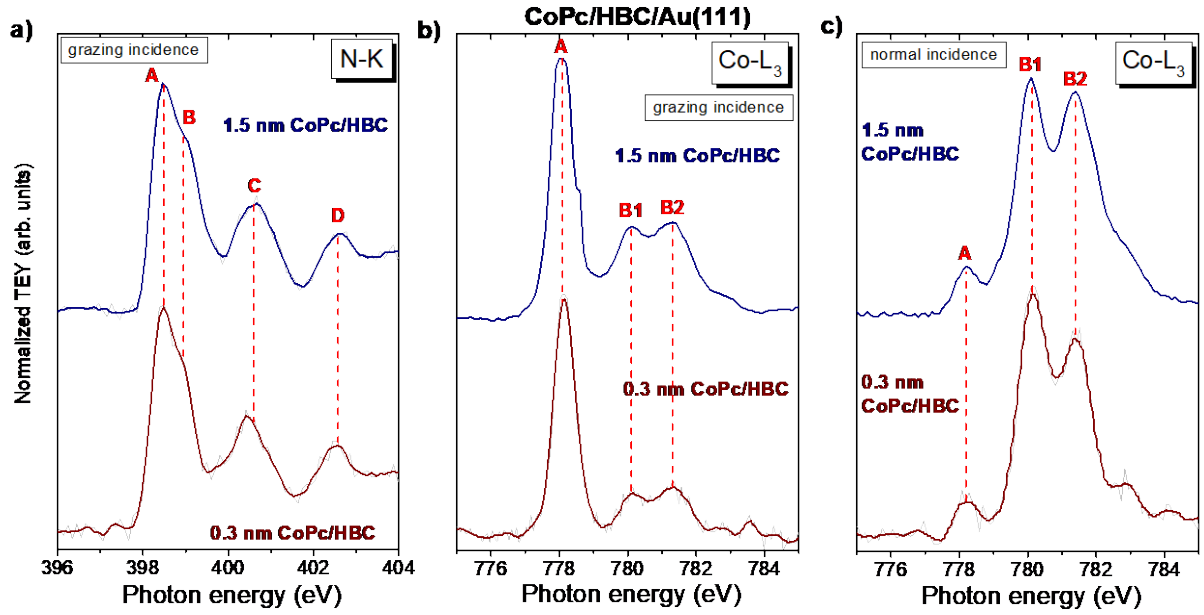

Figure 6. *Thickness-dependent N-K and Co-L_3 XAS of CoPc on a ML of HBC on Au(111): a) N-K at grazing incidence (10°), b) Co-L_3 at grazing incidence (10°), c) Co-L_3 at normal incidence (90°).*

In addition to the information about the molecular orientation in thin films, X-ray absorprtion spectra provide also valuable information about the electronic structure, in particular at interfaces. We will discuss changes of XAS peak shapes qualitatively, for a detailed discussion of the origin of features, we refer to the literature (e.g. Refs. [69-72]). In **Figure 6** we compare N-K edge

and Co-L_3 edge spectra for two different CoPc thicknesses on HBC/Au(111). Since the 0.3 nm layer corresponds to a coverage of about 1 ML, it represents information from the interface, whereas bulk-like spectra are obtained for the 1.5 nm thin film. The N-K edge spectra in **Figure 6a** are shown for grazing incidence of the incoming synchrotron light, exhibiting the maximal intensity of π^* resonances. Four different features denoted A-D can be distinguished, discussed in more detail in Refs. [34, 73]. Most important, there are only minuscule changes of the peak shape with film thickness, indicating that the nitrogen atoms are not involved to a significant amount to an interaction at the interface.

The Co-L_3 XA spectra in **Figures 6b** and **6c** show a complex fine structure, resulting from multiplet effects due to the strong overlap of the core wave function with the valence wave functions.[74] As a consequence, 16 transitions are possible for the absorption process $3d^7 \rightarrow 2p^5 3d^8$.[74] The different shape of Co-L_3 XAS at grazing and normal incidence in **Figures 6b** and **6c** arises from transitions into different d-orbitals (A: transitions into orbitals with out-of-plane components, B: transitions into orbitals with in-plane components). For both measurement geometries, changes of the shape of Co-L_3 XA spectra as a function of the film thickness are minor, indicating the absence of charge transfer to the central Co ion, as observed, e.g. for CoPc on gold-intercalated graphene/Ni(111).[8] In contrast, for CoPc deposited directly on different gold surfaces, distinct thickness dependent changes of both photoemission and XA spectra were observed, revealing an interfacial charge transfer.[34, 71, 75-76] The direct comparison to CoPc on Au(100) and Au foil suggests that the geometric structure of the considered Au surface has minor influence on electronic interface properties.[77] Thus, we conclude that the HBC intermediate layer can effectively prevent charge transfer from gold to CoPc.

This conclusion is confirmed by the corresponding $Co2p_{3/2}$, N1s and C1s XPS core level spectra, shown in **Figure 7** for two different thicknesses. Peak fit parameters for N1s and C1s spectra are summarized in **Tables S1-S4** (supporting information). All spectra of the bulk-like 2.7 nm CoPc thin film show the typical shape known from the literature.[8, 67, 78] The N1s signal is described by two components with same intensity ascribed to pyrrole (N1) and bridging nitrogen (N2) atoms. Because of their small energy separation (typically 0.3 - 0.5 eV for phthalocyanines[70, 79-83]), they cannot be clearly resolved by XPS. Two main components contribute to the C1s spectrum of the 2.7 nm thin film: Carbon bonded to nitrogen (C2) and carbon bonded to other carbon and hydrogen (C1). According to the fitting model described in Ref. [84], the main peaks are accompanied by their respective shake-up satellites, denoted S_{C1}, and S_{C2} in **Figure 7c.** The intensity ratio estimated from the peak areas $C1+S_{C1}$:$C2+S_{C2}$ of 3:1 matches perfectly to the stoichiometric composition (3:1).

Comparing the two film thicknesses, all core-level spectra for the lower coverages (0.3 nm) in **Figure 7** are shifted to 0.05 - 0.2 eV lower binding energies, which can be explained by screening effects of the photohole close to substrates with higher dielectric constants.[64, 77, 84-87]. However, most important, the shape of $Co2p_{3/2}$ and N1s core-level spectra in **Figure 7** is almost independent of the film thickness. In contrast, the $Co2p_{3/2}$ spectrum for a monolayer CoPc deposited directly on Au(111) exhibit a distinct interface component at 778.1 eV (the corresponding $Co2p_{3/2}$, N1s and C1s core level spectra are shown in **Figure S3**, supporting information). The small shoulder at the low binding energy side of the $Co2p_{3/2}$ spectrum of the 0.3 nm CoPc film on HBC covered Au(111) in **Figure 7a** at the energy of the interface component might arise from molecules at defect sites of the HBC layer, which may also explain the small

changes in the shape of the corresponding XAS. Furthermore, the peak fit analysis reveals that the apparent change of the shape of the C1s core-level spectra in **Figure 7c** is caused by a superposition of HBC and CoPc related features. Thus, the analysis of the thickness-dependent core level spectra confirms the absence of strong interactions like charge transfer at the interface to HBC/Au(111).

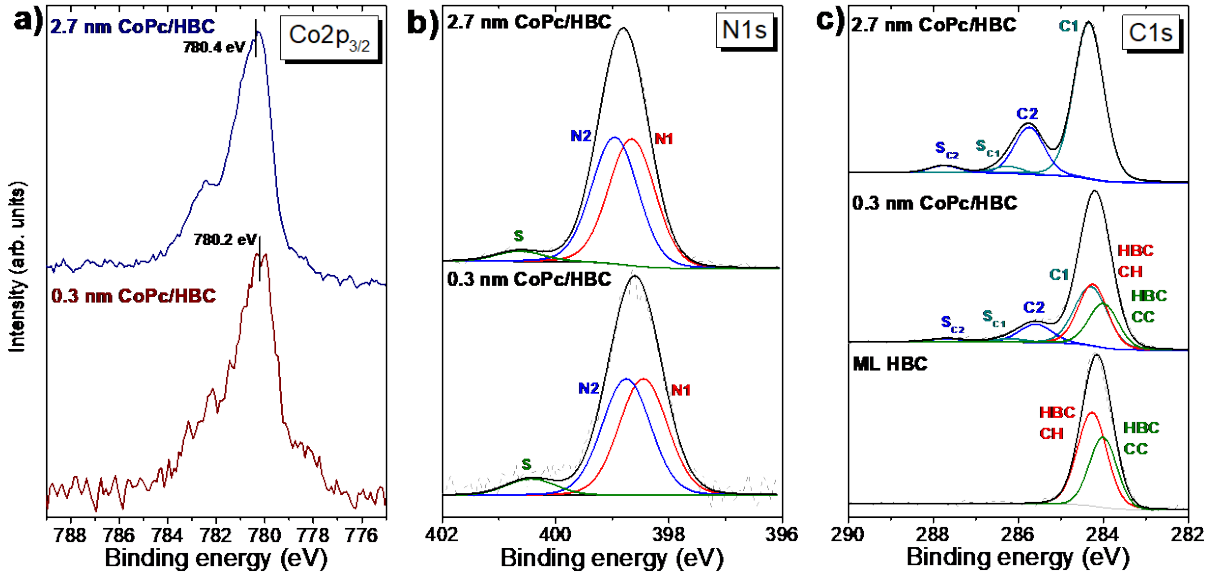

Figure 7. *Thickness-dependent core level spectra of CoPc on a ML of HBC on Au(111) with hν = 1486.7 eV: a) Co2p, b) N1s, c) C1s.*

Finally, the development of valence structures at the interface between CoPc and HBC/Au(111) was monitored as a function of CoPc film thickness. In **Figure 8**, we show the region of the highest occupied molecular orbital (HOMO) for HBC/Au(111) and two different CoPc thicknesses on HBC/Au(111). The spectrum of the clean Au (111) substrate is shown as a reference. The spectra were taken at an emission angle of 18.5° with respect to normal emission, which was chosen to achieve higher intensity from the molecular orbitals compared to normal emission. No features

within the first 2 eV relative to the Fermi-edge are visible in the reference spectrum of the Au(111) substrate in **Figure 8**. After the preparation of the HBC ML two features at 1.4 eV and 1.8 eV appear; the structure at 1.4 eV can be assigned to the HOMO of HBC.[20] After depositing 0.3 nm of CoPc on top, the intensity of the HBC-related feature at 1.4 eV becomes attenuated by the overlayer and a new peak at 1.0 eV appears. The binding energy of 1 eV is typical for the HOMO of CoPc for monolayer coverages on less reactive substrates.[71, 88] The HOMO of the 1.5 nm thin film shifts slightly by about 0.2 eV to 1.2 eV and thus, about the same amount as the core-levels, explained by screening effects of the photohole (see above). Interestingly, the HOMO of the bulk-like 1.5 nm film in **Figure 8** is clearly split into two features with maxima at 1.1 and 1.3 eV, which might arise from the electronic structure of CoPc.[70, 89] However, contributions from HBC cannot be fully excluded.

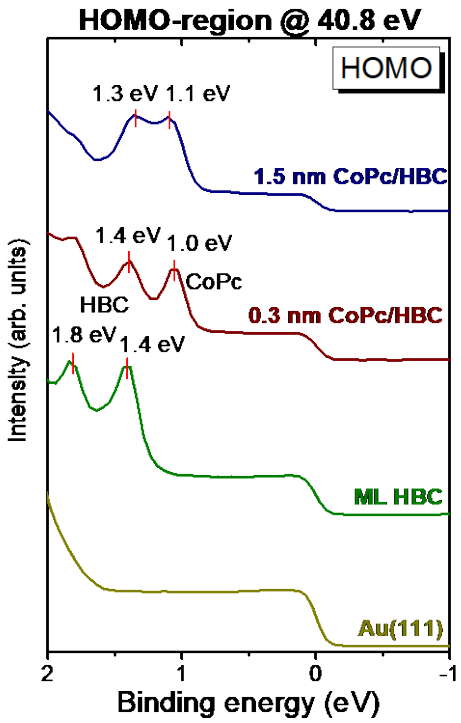

Figure 8. *HOMO-region measured after each deposition step and the clean Au(111) substrate at 40.8 eV and an emission angle of 18.5° with respect to normal emission.*

3.3. Temperature-induced Molecular Exchange

So far, we have demonstrated that the HBC intermediate layer can prevent interactions between CoPc and gold. In order to study whether this bilayer structure is stable against thermally induced rearrangement, we annealed CoPc/HBC/Au(111) samples to 630 K and performed PES, XAS and STM measurements.

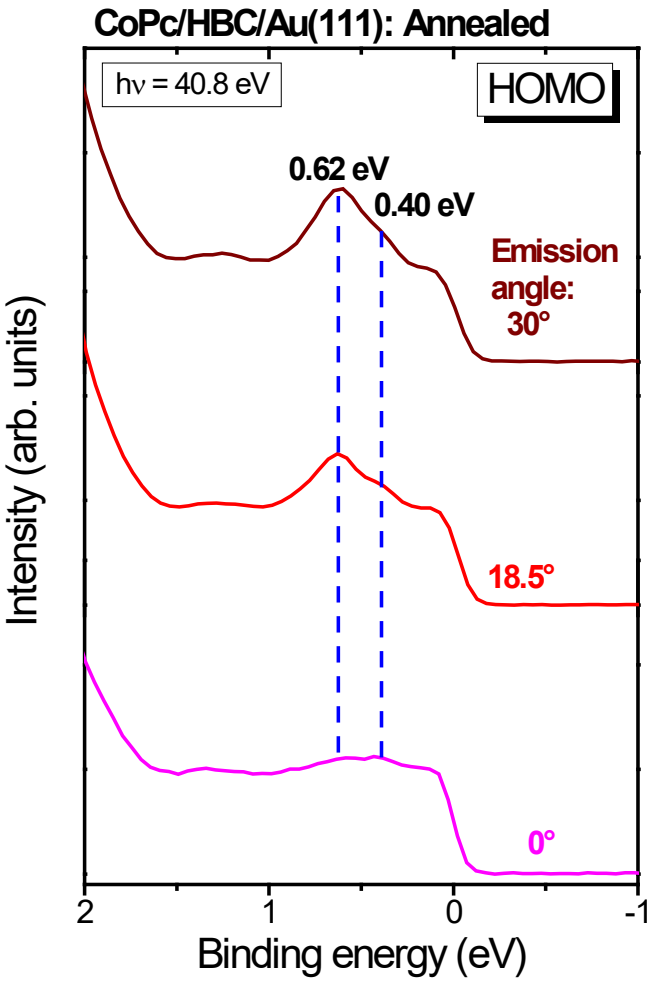

Figure 9. *Valence band spectra with zoom into the HOMO-region after annealing: as a function of emission angle (excitation energy 40.8 eV) with respect to normal emission.*

First, we will discuss photoemission valence band spectra (**Figure 9**) of an CoPc(1.5 nm)/HBC/Au(111) sample, annealed to 630 K. In contrast to the sample before annealing (cf. **Figure 8**), two new well-defined and intense states at 0.62 and 0.40 eV appear in the HOMO-region, while the former features at 1.3 and 1.1 eV are almost missing. Generally, the intensity of valence band features depends crucially on both the emission angle and the excitation energy (see, e.g. Refs. [78, 96-101]). Unfortunately, for both HBC-derivatives and phthalocyanines, the maximal intensity of the lowest lying valence band features is expected around 1.5-1.7 $Å^{-1}$,[78, 98-101] and thus it is difficult to distinguish between both molecules from angular dependent intensity variations.

The intensity of features at binding energies of 0.40 and 0.62 eV in **Figures 9a** increases with higher polar angle; they are most intense at 30°, which corresponds to $k_{||} \sim 1.5$ $Å^{-1}$. Since such a behavior is expected for valence band features of CoPc and HBC, we conclude that the interface states can be assigned to molecular orbitals, most likely to the HOMO of CoPc and/or HBC. The fact that they are observed at distinctly lower binding energy compared to the HOMO before annealing (cf. **Figure 8**) may point to a strong coupling to the substrate.

We would like to emphasize, that these states do not simply originate from a rigid shift of photoemission features due to screening or a variation of the energy level alignment, since no related shift were observed in the corresponding C1s core levels (0.1-0.25 eV to lower binding energy in various experiments). We note that the shape of the valence band spectrum is very similar to CoPc on Au(111) (cf. **Figure S4**, supporting information), suggesting that the HOMO of CoPc contributes significantly.

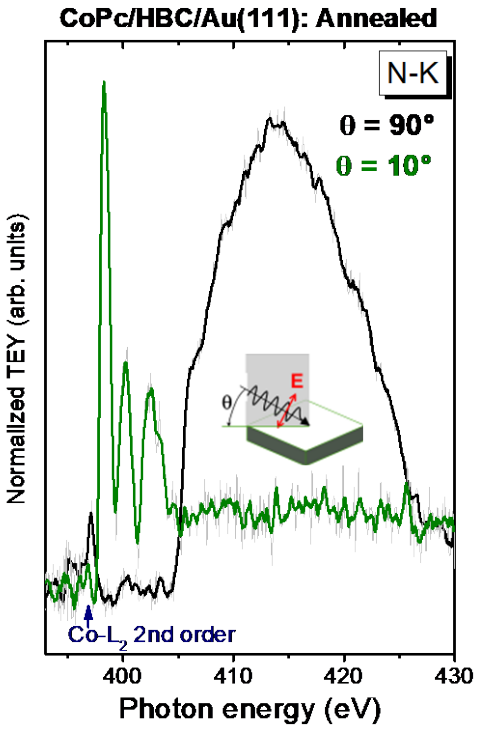

Figure 10. *Angle-dependent N-K XA spectra of CoPc/HBC/Au(111) after annealing to 630 K.*

As already mentioned, distinct changes of the XAS peak shape are expected for CoPc molecules in direct contact to reactive substrates. In **Figure 10**, we show angle dependent N-K edge XA spectra of the CoPc/HBC/Au(111) sample after annealing. The angular dependence indicates that CoPc molecules remain flat lying after annealing. The almost vanished intensity in the π*-region at grazing incidence points to an almost perfect orientation parallel to the substrate surface. However, the N-K peak shape is very similar to the sample before annealing (cf. **Figure 5**). This indicates that nitrogen atoms of CoPc are not involved in a possible strong interaction at the interface to Au(111), as might be expected even for CoPc molecules in direct contact to Au.[71]

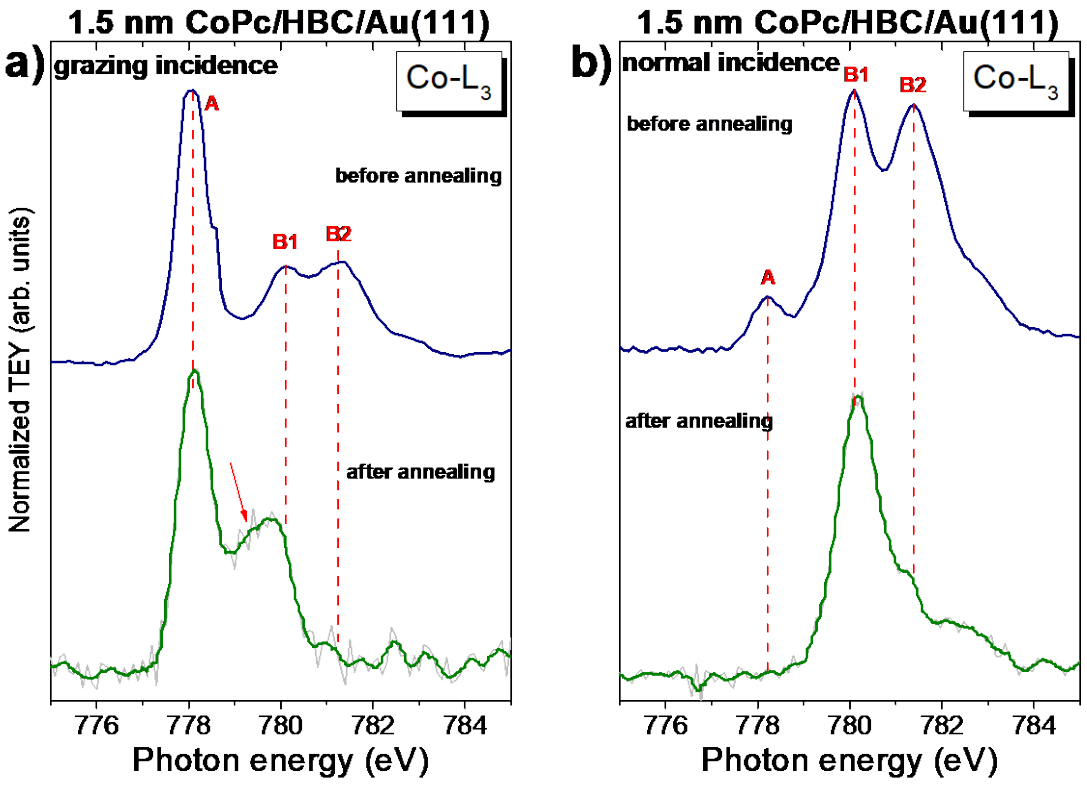

Figure 11. *Angle-dependent Co-L_3 XA spectra of CoPc(1.5 nm)/HBC/Au(111) after annealing to 630 K (green curves) compared to the same sample before annealing (blue curves) taken at grazing (10°) and normal incidence (90°) of the incoming p-polarized synchrotron light.*

In contrast, the shape of Co-L_3 XA spectra in **Figure 11** is clearly different comparing the 1.5 nm CoPc layer on HBC/Au(111) before and after annealing to 630 K. Most visible, the prominent feature B2 substantially drops in intensity after annealing in the spectra taken at grazing and normal incidence. Also, the shape of feature A changes slightly and additional intensity is observed at higher photon energies (red arrow in **Figure 11a**). The changes of the peak shape indicate a charge transfer from the substrate to the Co ion of CoPc, accompanied by a redistribution of the d-electrons. Such a behavior is typical for CoPc in direct contact to Au.[71, 75]

Thus, we conclude from Co-L_3 XA spectra that the interaction between CoPc and Au is no longer prevented by an HBC intermediate layer, the CoPc molecules are most likely diffused to the Au(111) interface upon annealing.

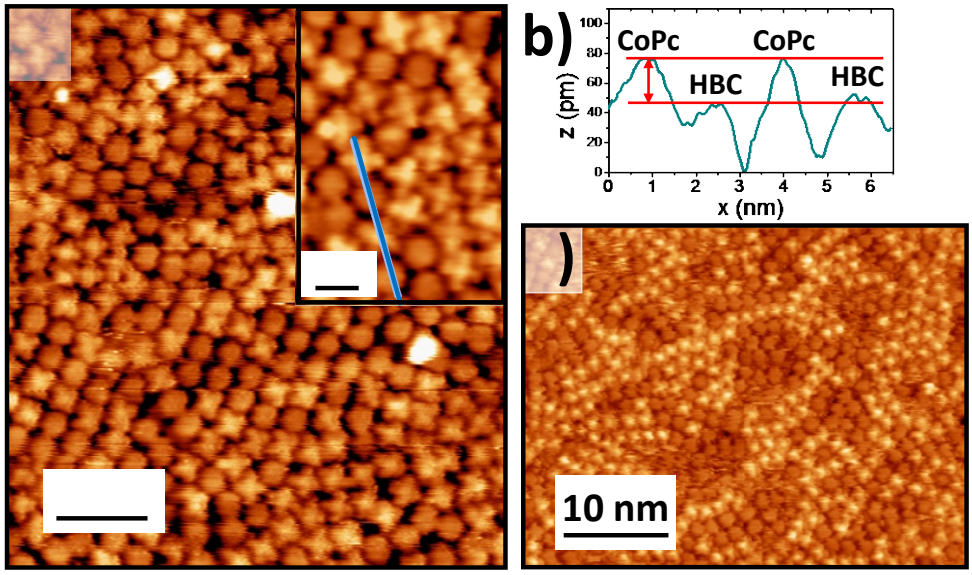

Figure 12. *STM images of CoPc/HBC/Au(111), annealed to 630 K. a) 25 · 28 nm² image (U = 1.5 V, I = 950 pA). The inset shows a close-up measured with the same parameters, used for the line profile shown in b). c) 45 · 35 nm² image (U = 1.0 V and I = 800 pA). CoPc molecules are visible as bright spots.*

The question may arise as to whether CoPc molecules replace the HBC molecules at the interface after annealing completely. Therefore, we performed STM measurements of the annealed CoPc/HBC/Au(111) sample. Two different molecular structures can be identified in the STM images of **Figure 12**. The four-leaved pattern, typical for phthalocyanines, is best visible for some molecules in **Figure 12a**, for other molecules a hexagonal structure typical for HBC might be

supposed. The CoPc molecules appear somewhat brighter than the HBC molecules in **Figure 12a** (bias voltage of + 1.5 V). This effect is more pronounced in **Figure 12c**, at a bias voltage of + 1.0 V. This effect is might be caused by the increased brightness of the central Co-atom due to enhanced tunneling via the half-filled d_{z^2} orbitals at this tunneling voltage.[103] Due to the local density of molecular states of the d-orbitals, the central metal atoms of TMPcs have higher apparent heights than the macrocycle.[103-104] Therefore, depending on the tunneling voltage, we can distinguish between CoPc and HBC molecules by their apparent height. A line profile is generated from the close-up of **Figure 12a** (inset), illustrated in **Figure 12b**. The line profile reveals a height difference between the CoPc and HBC molecules of about 30 pm. From the slight differences in the apparent height, we conclude that the CoPc and HBC molecules are almost at the same level on Au(111), i.e. they form a mixed monolayer on Au(111).

Often bimolecular layers form ordered structures due to molecule – molecule interaction by H-bonds, dipole-dipole interaction or metal coordination.[105-109] In **Figure 12,** it seems that molecules of the same type (CoPc or HBC) tend to form domains, but also a large number of single molecules and irregular spaces between the molecules (dark areas) are visible. Consequently, we could not identify a preferred ordering as discussed for CoPc and HBC monolayers on Au(111) (cf. **Figure 2-4**). This is supported by the absence of a LEED pattern, shown in **Figure S2**.

Thus, our results verify that a molecular rearrangement and exchange takes place in the monolayer after annealing of CoPc(1.5 nm)/HBC/Au(111). However, not all of the CoPc molecules are able to replace HBC molecules at the interface to Au(111) at the selected experimental conditions. Obviously, the interactions between CoPc molecules are weak enough to enable the

desorption of CoPc at the chosen temperature of 630 K. Possibly, a temperature-induced intermixing at the HBC/CoPc interface likely driven by entropy might occur in parallel to the thermal desorption from the top layers until a mixed monolayer film remains on the surface.

Alternatively, the progressive CoPc desorption from the top layers of the film may leave some HBC molecules directly exposed to vacuum. In this case, also HBC desorption might happen in parallel to desorption but also diffusion and sticking of CoPc at former HBC adsorption sites, which again will lead to an intermixed layer. We note that the detailed composition of the remaining, mixed HBC-CoPc monolayer may strongly depend on both the desorption kinetics of CoPc and the kinetics of the diffusion/exchange. Therefore, we suggest that especially the variation of the temperature regime enables the tuning of the arrangement of molecules and their composition in the mixed layer.

4. Conclusion

We studied interface properties and the structural ordering of cobalt phthalocyanine (CoPc) on a highly ordered monolayer (ML) hexa-*peri*-hexabenzocoronene (HBC), grown on Au(111). LEED and STM measurements reveal that well-ordered CoPc layers are formed on HBC/Au(111). The HBC layer acts as a template for the initial growth of CoPc molecules. An hexagonal arrangement is observed for CoPc on HBC/Au(111); the angle between the lattice vectors is the same as for the annealed HBC monolayer ($\Gamma = 60°$). A charge transfer between CoPc and the gold substrate is almost completely prevented by the HBC intermediate layer. After annealing to 630 K, a molecular exchange takes place and a mixed monolayer of CoPc and HBC is formed on the

Au(111) substrate. We conclude that the interaction strength between CoPc and Au(111) is not significantly stronger compared to HBC/Au(111).

Acknowledgements

The authors thank the Helmholtz-Zentrum Berlin (HZB) for the allocation of synchrotron radiation. Financial travel support by HZB is thankfully acknowledged. The Center for Light-Matter Interaction, Sensors & Analytics (LISA$^+$) at the University of Tübingen is acknowledged for technical support. We thank Prof. H.F. Bettinger (Tübingen) for valuable discussions and the synthesis of HBC.

ASSOCIATED CONTENT

Supporting Information

- Large scale STM images.
- LEED pattern of CoPc/HBC/Au(111) after annealing to 630 K.
- XPS core level spectra for a monolayer (0.3 nm) CoPc on Au(111).
- Valence band spectra of CoPc/HBC/Au(111) compared to CoPc/Au(111).
- Peakfit parameters.

References

1. Koch, N., Organic electronic devices and their functional interfaces. *ChemPhysChem* **2007,** *8* (10), 1438-1455.
2. Ma, H.; Yip, H. L.; Huang, F.; Jen, A. K. Y., Interface Engineering for Organic Electronics. *Adv. Funct. Mater.* **2010,** *20* (9), 1371-1388.

3. Sanvito, S., Molecular spintronics. *Chemical Society Reviews* **2011,** *40* (6), 3336-3355.
4. Forrest, S. R., The path to ubiquitous and low-cost organic electronic appliances on plastic. *Nature* **2004,** *428* (6986), 911-918.
5. Dodabalapur, A.; Katz, H. E.; Torsi, L.; Haddon, R. C., Organic Heterostructure Field-ÈffectTransistors. *Science* **1995,** *269* (5230), 1560.
6. Tang, C. W., Two-layer organic photovoltaic cell. *Applied Physics Letters* **1986,** *48* (2), 183-185.
7. Katz, H. E.; Lovinger, A. J.; Johnson, J.; Kloc, C.; Siegrist, T.; Li, W.; Lin, Y. Y.; Dodabalapur, A., A soluble and air-stable organic semiconductor with high electron mobility. *Nature* **2000,** *404* (6777), 478-481.
8. Uihlein, J.; Polek, M.; Glaser, M.; Adler, H.; Ovsyannikov, R.; Bauer, M.; Ivanovic, M.; Preobrajenski, A. B.; Generalov, A. V.; Chassé, T.; Peisert, H., Influence of Graphene on Charge Transfer between CoPc and Metals: The Role of Graphene–Substrate Coupling. *J. Phys. Chem. C* **2015,** *119* (27), 15240-15247.
9. Balle, D.; Adler, H.; Grüninger, P.; Karstens, R.; Ovsyannikov, R.; Giangrisostomi, E.; Chassé, T.; Peisert, H., Influence of the Fluorination of CoPc on the Interfacial Electronic Structure of the Coordinated Metal Ion. *J. Phys. Chem. C* **2017,** *121* (34), 18564-18574.
10. Ameri, T.; Li, N.; Brabec, C. J., Highly efficient organic tandem solar cells: a follow up review. *Energy & Environmental Science* **2013,** *6* (8), 2390-2413.
11. Chung, K.; Lee, C.-H.; Yi, G.-C., Transferable GaN Layers Grown on ZnO-Coated Graphene Layers for Optoelectronic Devices. *Science* **2010,** *330* (6004), 655.
12. Kawasaki, T.; Ichimura, T.; Kishimoto, H.; Akbar, A. A.; Ogawa, T.; Oshima, C., DOUBLE ATOMIC LAYERS OF GRAPHENE/MONOLAYER h-BN ON Ni(111) STUDIED BY SCANNING TUNNELING MICROSCOPY AND SCANNING TUNNELING SPECTROSCOPY. *Surface Review and Letters* **2002,** *09* (03n04), 1459-1464.
13. Scarfato, A.; Chang, S.-H.; Kuck, S.; Brede, J.; Hoffmann, G.; Wiesendanger, R., Scanning tunneling microscope study of iron(II) phthalocyanine growth on metals and insulating surfaces. *Surface Science* **2008,** *602* (3), 677-683.
14. Dahal, A.; Batzill, M., Graphene–nickel interfaces: a review. *Nanoscale* **2014,** *6* (5), 2548-2562.
15. Wintterlin, J.; Bocquet, M. L., Graphene on metal surfaces. *Surface Science* **2009,** *603* (10), 1841-1852.
16. Nie, S.; Bartelt, N. C.; Wofford, J. M.; Dubon, O. D.; McCarty, K. F.; Thürmer, K., Scanning tunneling microscopy study of graphene on Au(111): Growth mechanisms and substrate interactions. *Physical Review B* **2012,** *85* (20), 205406.
17. Oznuluer, T.; Pince, E.; Polat, E. O.; Balci, O.; Salihoglu, O.; Kocabas, C., Synthesis of graphene on gold. *Applied Physics Letters* **2011,** *98* (18), 183101.
18. Grimsdale, A. C.; Wu, J.; Mullen, K., New carbon-rich materials for electronics, lithium battery, and hydrogen storage applications. *Chem. Commun.* **2005,** (17), 2197-2204.
19. Helga, S.; Balaji, P.; David, J. J.; Andrew, B. H.; Wallace, W. H. W., Hexa-peri-hexabenzocoronene in organic electronics. *Pure and Applied Chemistry* **2012,** *84* (4), 1047-1067.
20. Proehl, H.; Toerker, M.; Sellam, F.; Fritz, T.; Leo, K.; Simpson, C.; Müllen, K., Comparison of ultraviolet photoelectron spectroscopy and scanning tunneling spectroscopy measurements on highly ordered ultrathin films of hexa-peri-hexabenzocoronene on Au(111). *Physical Review B* **2001,** *63* (20), 205409.
21. Sellam, F.; Schmitz-Hübsch, T.; Toerker, M.; Mannsfeld, S.; Proehl, H.; Fritz, T.; Leo, K.; Simpson, C.; Müllen, K., LEED and STM investigations of organic–organic heterostructures grown by molecular beam epitaxy. *Surf. Sci.* **2001,** *478* (1), 113-121.
22. Ruffieux, P.; Gröning, O.; Bielmann, M.; Simpson, C.; Müllen, K.; Schlapbach, L.; Gröning, P., Supramolecular columns of hexabenzocoronenes on copper and gold (111) surfaces. *Phys. Rev. B* **2002,** *66* (7), 073409.

23. Belser, A.; Greulich, K.; Grüninger, P.; Bettinger, H. F.; Peisert, H.; Chassé, T., Visualization of the Borazine Core of B_3N_3-Doped Nanographene by STM. *ACS Appl. Mater. Interfaces* **2020,** *12* (16), 19218-19225.
24. Amsalem, P.; Wilke, A.; Frisch, J.; Niederhausen, J.; Vollmer, A.; Rieger, R.; Müllen, K.; Rabe, J. P.; Koch, N., Interlayer molecular diffusion and thermodynamic equilibrium in organic heterostructures on a metal electrode. *Journal of Applied Physics* **2011,** *110* (11), 113709.
25. Duhm, S.; Salzmann, I.; Bröker, B.; Glowatzki, H.; Johnson, R. L.; Koch, N., Interdiffusion of molecular acceptors through organic layers to metal substrates mimics doping-related energy level shifts. *Applied Physics Letters* **2009,** *95* (9), 093305.
26. Sun, L.; Liu, C.; Queteschiner, D.; Weidlinger, G.; Zeppenfeld, P., Layer inversion in organic heterostructures. *Phys. Chem. Chem. Phys.* **2011,** *13* (29), 13382-13386.
27. Gallego, J. M.; Ecija, D.; Martín, N.; Otero, R.; Miranda, R., An STM study of molecular exchange processes in organic thin film growth. *Chemical Communications* **2014,** *50* (69), 9954-9957.
28. Stadtmüller, B.; Gruenewald, M.; Peuker, J.; Forker, R.; Fritz, T.; Kumpf, C., Molecular Exchange in a Heteromolecular PTCDA/CuPc Bilayer Film on Ag(111). *The Journal of Physical Chemistry C* **2014,** *118* (49), 28592-28602.
29. Wang, Q.; Yang, J. C.; Franco-Canellas, A.; Burker, C.; Niederhausen, J.; Dombrowski, P.; Widdascheck, F.; Breuer, T.; Witte, G.; Gerlach, A.; Duhm, S.; Schreiber, F., Pentacene/perfluoropentacene bilayers on Au(111) and Cu(111): impact of organic-metal coupling strength on molecular structure formation. *Nanoscale Advances* **2021,** *3* (9), 2598-2606.
30. Gruenewald, M.; Sauer, C.; Peuker, J.; Meissner, M.; Sojka, F.; Schöll, A.; Reinert, F.; Forker, R.; Fritz, T., Commensurism at electronically weakly interacting phthalocyanine/PTCDA heterointerfaces. *Phys. Rev. B* **2015,** *91* (15), 155432.
31. Kleimann, C.; Stadtmüller, B.; Schröder, S.; Kumpf, C., Electrostatic interaction and commensurate registry at the heteromolecular F16CuPc–CuPc interface. *J. Phys. Chem. C* **2014,** *118* (3), 1652-1660.
32. Häming, M.; Greif, M.; Sauer, C.; Schöll, A.; Reinert, F., Electronic structure of ultrathin heteromolecular organic-metal interfaces: SnPc/PTCDA/Ag(111) and SnPc/Ag(111). *Physical Review B* **2010,** *82* (23), 235432.
33. Borghetti, P.; de Oteyza, D. G.; Rogero, C.; Goiri, E.; Verdini, A.; Cossaro, A.; Floreano, L.; Ortega, J. E., Molecular-Level Realignment in Donor–Acceptor Bilayer Blends on Metals. *The Journal of Physical Chemistry C* **2016,** *120* (11), 5997-6005.
34. Peisert, H.; Uihlein, J.; Petraki, F.; Chassé, T., Charge transfer between transition metal phthalocyanines and metal substrates: The role of the transition metal. *J. Electron Spectros. Relat. Phenomena* **2015,** *204*, 49-60.
35. Rehman, R. A.; Zhang, H. J.; Razaq, A.; Ramay, S. M.; Hasan, M.; Javed, M. A.; Atiq, S., Spectro-microscopy characterization of CoPc-Au(111) interface. *Physica E-Low-Dimensional Systems & Nanostructures* **2021,** *125*.
36. Liu, R.; Wu, D.; Feng, X.; Müllen, K., Bottom-up fabrication of photoluminescent graphene quantum dots with uniform morphology. *J. Am. Chem. Soc.* **2011,** *133* (39), 15221-15223.
37. Yeh, J. J.; Lindau, I., ATOMIC SUBSHELL PHOTOIONIZATION CROSS-SECTIONS AND ASYMMETRY PARAMETERS - 1 LESS-THAN-OR-EQUAL-TO Z LESS-THAN-OR-EQUAL-TO 103. *Atom. Data Nucl. Data Tables* **1985,** *32* (1), 1-155.
38. Seah, M. P.; Dench, W. A., Quantitative electron spectroscopy of surfaces: A standard data base for electron inelastic mean free paths in solids. *Surf. Interface Anal.* **1979,** *1* (1), 2-11.
39. Horcas, I.; Fernández, R.; Gómez-Rodríguez, J. M.; Colchero, J.; Gómez-Herrero, J.; Baro, A. M., WSXM: A software for scanning probe microscopy and a tool for nanotechnology. *Review of Scientific Instruments* **2007,** *78* (1), 013705.

40. Hesse, R.; Chasse, T.; Streubel, P.; Szargan, R., Error estimation in peak-shape analysis of XPS core-level spectra using UNIFIT 2003: how significant are the results of peak fits? *Surf. Interface Anal.* **2004,** *36* (10), 1373-1383.
41. Giangrisostomi, E.; Ovsyannikov, R.; Sorgenfrei, F.; Zhang, T.; Lindblad, A.; Sassa, Y.; Cappel, U. B.; Leitner, T.; Mitzner, R.; Svensson, S.; Mårtensson, N.; Föhlisch, A., Low Dose Photoelectron Spectroscopy at BESSY II: Electronic structure of matter in its native state. *J. Electron Spectros. Relat. Phenomena* **2018,** *224*, 68-78.
42. Vollmer, A.; Ovsyannikov, R.; Gorgoi, M.; Krause, S.; Oehzelt, M.; Lindblad, A.; Martensson, N.; Svensson, S.; Karlsson, P.; Lundvuist, M.; Schmeiler, T.; Pflaum, J.; Koch, N., Two dimensional band structure mapping of organic single crystals using the new generation electron energy analyzer ARTOF. *J. Electron Spectros. Relat. Phenomena* **2012,** *185* (3-4), 55-60.
43. Schreiber, F., Organic molecular beam deposition: Growth studies beyond the first monolayer. *Phys Status Solidi A* **2004,** *201* (6), 1037-1054.
44. Peisert, H.; Biswas, I.; Knupfer, M.; Chasse, T., Orientation and electronic properties of phthalocyanines on polycrystalline substrates. *Phys Status Solidi B* **2009,** *246* (7), 1529-1545.
45. Novák, J.; Oehzelt, M.; Berkebile, S.; Koini, M.; Ules, T.; Koller, G.; Haber, T.; Resel, R.; Ramsey, M. G., Crystal growth of para-sexiphenyl on clean and oxygen reconstructed Cu (110) surfaces. *Phys. Chem. Chem. Phys.* **2011,** *13* (32), 14675-14684.
46. Wagner, C.; Kasemann, D.; Golnik, C.; Forker, R.; Esslinger, M.; Müllen, K.; Fritz, T., Repulsion between molecules on a metal: Monolayers and submonolayers of hexa-peri-hexabenzocoronene on Au(111). *Phys. Rev. B* **2010,** *81* (3), 035423.
47. Liu, L.; Yu, J.; Viernes, N. O. L.; Moore, J. S.; Lyding, J. W., Adsorption of cobalt phthalocyanine on Si(100)2×1 and Si(100)2×1:H surfaces studied by scanning tunneling microscopy and spectroscopy. *Surface Science* **2002,** *516* (1), 118-126.
48. Barlow, D. E.; Scudiero, L.; Hipps, K. W., Scanning Tunneling Microscopy Study of the Structure and Orbital-Mediated Tunneling Spectra of Cobalt(II) Phthalocyanine and Cobalt(II) Tetraphenylporphyrin on Au(111): Mixed Composition Films. *Langmuir* **2004,** *20* (11), 4413-4421.
49. Walzer, K.; Hietschold, M., STM and STS investigation of ultrathin tin phthalocyanine layers adsorbed on HOPG(0001) and Au(111). *Surface Science* **2001,** *471* (1), 1-10.
50. Lackinger, M.; Hietschold, M., Determining adsorption geometry of individual tin–phthalocyanine molecules on Ag(111)—a STM study at submonolayer coverage. *Surface Science* **2002,** *520* (1), L619-L624.
51. Kothe, M.; Witte, G., Orientational and Crystalline Order of Copper-Phthalocyanine Films on Gold: the Role of Substrate Roughness and Cleanliness. *Langmuir* **2019,** *35* (42), 13570-13577.
52. Gopakumar, T. G.; Lackinger, M.; Hackert, M.; Müller, F.; Hietschold, M., Adsorption of Palladium Phthalocyanine on Graphite: STM and LEED Study. *The Journal of Physical Chemistry B* **2004,** *108* (23), 7839-7843.
53. Buchholz, J. C.; Somorjai, G. A., The surface structures of phthalocyanine monolayers and vapor-grown films: A low-energy electron diffraction study. *The Journal of Chemical Physics* **1977,** *66* (2), 573-580.
54. England, C.; Collins, G.; Schuerlein, T.; Armstrong, N. R., Epitaxial thin films of large organic molecules: characterization of phthalocyanine and coronene overlayers on the layered semiconductors MoS2 and SnS2. *Langmuir* **1994,** *10* (8), 2748-2756.
55. Hämäläinen, S. K.; Stepanova, M.; Drost, R.; Liljeroth, P.; Lahtinen, J.; Sainio, J., Self-Assembly of Cobalt-Phthalocyanine Molecules on Epitaxial Graphene on Ir(111). *The Journal of Physical Chemistry C* **2012,** *116* (38), 20433-20437.
56. Jarvinen, P.; Hamalainen, S. K.; Ijas, M.; Harju, A.; Liljeroth, P., Self-Assembly and Orbital Imaging of Metal Phthalocyanines on a Graphene Model Surface. *J. Phys. Chem. C* **2014,** *118* (24), 13320-13325.

57. Barlow, D. E.; Hipps, K. W., A Scanning Tunneling Microscopy and Spectroscopy Study of Vanadyl Phthalocyanine on Au(111): the Effect of Oxygen Binding and Orbital Mediated Tunneling on the Apparent Corrugation. *The Journal of Physical Chemistry B* **2000,** *104* (25), 5993-6000.
58. Yamane, H.; Kosugi, N., Site-specific intermolecular valence-band dispersion in α-phase crystalline films of cobalt phthalocyanine studied by angle-resolved photoemission spectroscopy. *J. Chem. Phys.* **2014,** *141* (22), 224701.
59. Cheng, Z. H.; Gao, L.; Deng, Z. T.; Jiang, N.; Liu, Q.; Shi, D. X.; Du, S. X.; Guo, H. M.; Gao, H. J., Adsorption Behavior of Iron Phthalocyanine on Au(111) Surface at Submonolayer Coverage. *J. Phys. Chem. C* **2007,** *111* (26), 9240-9244.
60. Yoshimoto, S.; Tada, A.; Suto, K.; Itaya, K., Adlayer Structures and Electrocatalytic Activity for O2 of Metallophthalocyanines on Au(111): In Situ Scanning Tunneling Microscopy Study. *The Journal of Physical Chemistry B* **2003,** *107* (24), 5836-5843.
61. Yoshimoto, S.; Higa, N.; Itaya, K., Two-Dimensional Supramolecular Organization of Copper Octaethylporphyrin and Cobalt Phthalocyanine on Au(111): Molecular Assembly Control at an Electrochemical Interface. *Journal of the American Chemical Society* **2004,** *126* (27), 8540-8545.
62. Chizhov, I.; Scoles, G.; Kahn, A., The Influence of Steps on the Orientation of Copper Phthalocyanine Monolayers on Au(111). *Langmuir* **2000,** *16* (9), 4358-4361.
63. England, C.; Collins, G.; Schuerlein, T.; Armstrong, N., Epitaxial thin films of large organic molecules: characterization of phthalocyanine and coronene overlayers on the layered semiconductors MoS2 and SnS2. *Langmuir* **1994,** *10* (8), 2748-2756.
64. Belser, A.; Karstens, R.; Nagel, P.; Merz, M.; Schuppler, S.; Chassé, T.; Peisert, H., Interaction Channels Between Perfluorinated Iron Phthalocyanine and Cu(111). *physica status solidi (b)* **2019,** *256* (2), 1800292.
65. Greulich, K.; Belser, A.; Bölke, S.; Grüninger, P.; Karstens, R.; Sättele, M. S.; Ovsyannikov, R.; Giangrisostomi, E.; Basova, T. V.; Klyamer, D. D.; Chassé, T.; Peisert, H., Charge Transfer from Organic Molecules to Molybdenum Disulfide: Influence of the Fluorination of Iron Phthalocyanine. *J. Phys. Chem. C* **2020,** *124* (31), 16990-16999.
66. Karstens, R.; Glaser, M.; Belser, A.; Balle, D.; Polek, M.; Ovsyannikov, R.; Giangrisostomi, E.; Chasse, T.; Peisert, H., FePc and FePcF16 on Rutile TiO2(110) and (100): Influence of the Substrate Preparation on the Interaction Strength. *Molecules* **2019,** *24* (24), 20.
67. Scardamaglia, M.; Struzzi, C.; Lizzit, S.; Dalmiglio, M.; Lacovig, P.; Baraldi, A.; Mariani, C.; Betti, M. G., Energetics and Hierarchical Interactions of Metal Phthalocyanines Adsorbed on Graphene/Ir(111). *Langmuir* **2013,** *29* (33), 10440-10447.
68. Lindner, S.; Treske, U.; Knupfer, M., The complex nature of phthalocyanine/gold interfaces. *Appl. Surf. Sci.* **2013,** *267*, 62-65.
69. Zhang, T.; Brumboiu, I. E.; Lanzilotto, V.; Luder, J.; Grazioli, C.; Giangrisostomi, E.; Ovsyannikov, R.; Sass, Y.; Bidermane, I.; Stupar, M.; de Simone, M.; Coreno, M.; Ressel, B.; Pedio, M.; Rudolf, P.; Brena, B.; Puglia, C., Conclusively Addressing the CoPc Electronic Structure: A Joint Gas-Phase and Solid-State Photoemission and Absorption Spectroscopy Study. *J. Phys. Chem. C* **2017,** *121* (47), 26372-26378.
70. Maslyuk, V. V.; Aristov, V. Y.; Molodtsova, O. V.; Vyalikh, D. V.; Zhilin, V. M.; Ossipyan, Y. A.; Bredow, T.; Mertig, I.; Knupfer, M., The electronic structure of cobalt phthalocyanine. *Appl Phys a-Mater* **2009,** *94* (3), 485-489.
71. Betti, M. G.; Gargiani, P.; Frisenda, R.; Biagi, R.; Cossaro, A.; Verdini, A.; Floreano, L.; Mariani, C., Localized and Dispersive Electronic States at Ordered FePc and CoPc Chains on Au(110). *J. Phys. Chem. C* **2010,** *114* (49), 21638-21644.

72. Kroll, T.; Aristov, V. Y.; Molodtsova, O. V.; Ossipyan, Y. A.; Vyalikh, D. V.; Buchner, B.; Knupfer, M., Spin and orbital ground state of Co in cobalt phthalocyanine. *J. Phys. Chem. A* **2009,** *113* (31), 8917-8922.
73. Willey, T. M.; Bagge-Hansen, M.; Lee, J. R. I.; Call, R.; Landt, L.; van Buuren, T.; Colesniuc, C.; Monton, C.; Valmianski, I.; Schuller, I. K., Electronic structure differences between H-2-, Fe-, Co-, and Cu-phthalocyanine highly oriented thin films observed using NEXAFS spectroscopy. *J. Chem. Phys.* **2013,** *139* (3).
74. de Groot, F., Multiplet effects in X-ray spectroscopy. *Coord. Chem. Rev.* **2005,** *249* (1-2), 31-63.
75. Petraki, F.; Peisert, H.; Biswas, I.; Aygul, U.; Latteyer, F.; Vollmer, A.; Chasse, T., Interaction between Cobalt Phthalocyanine and Gold Studied by X-ray Absorption and Resonant Photoemission Spectroscopy. *J Phys Chem Lett* **2010,** *1* (23), 3380-3384.
76. Gargiani, P.; Rossi, G.; Biagi, R.; Corradini, V.; Pedio, M.; Fortuna, S.; Calzolari, A.; Fabris, S.; Cezar, J. C.; Brookes, N. B.; Betti, M. G., Spin and orbital configuration of metal phthalocyanine chains assembled on the Au(110) surface. *Phys Rev B* **2013,** *87* (16), 165407.
77. Petraki, F.; Peisert, H.; Biswas, I.; Chasse, T., Electronic Structure of Co-Phthalocyanine on Gold Investigated by Photoexcited Electron Spectroscopies: Indication of Co Ion-Metal Interaction. *J. Phys. Chem. C* **2010,** *114* (41), 17638-17643.
78. Yamane, H.; Kosugi, N., Site-specific organic/metal interaction revealed from shockley-type interface state. *J. Phys. Chem. C* **2016,** *120* (42), 24307-24313.
79. Evangelista, F.; Ruocco, A.; Gotter, R.; Cossaro, A.; Floreano, L.; Morgante, A.; Crispoldi, F.; Betti, M. G.; Mariani, C., Electronic states of CuPc chains on the Au(110) surface. *J. Chem. Phys.* **2009,** *131* (17), 174710.
80. Papageorgiou, N.; Ferro, Y.; Salomon, E.; Allouche, A.; Layet, J. M.; Giovanelli, L.; Le Lay, G., Geometry and electronic structure of lead phthalocyanine: Quantum calculations via density-functional theory and photoemission measurements. *Phys. Rev. B* **2003,** *68* (23), 235105.
81. Papageorgiou, N.; Salomon, E.; Angot, T.; Layet, J.-M.; Giovanelli, L.; Lay, G. L., Physics of ultra-thin phthalocyanine films on semiconductors. *Prog. Surf. Sci.* **2004,** *77* (5), 139-170.
82. Schmid, M.; Kaftan, A.; Steinruck, H. P.; Gottfried, J. M., The electronic structure of cobalt(II) phthalocyanine adsorbed on Ag(111). *Surf. Sci.* **2012,** *606* (11-12), 945-949.
83. Åhlund, J.; Nilson, K.; Schiessling, J.; Kjeldgaard, L.; Berner, S.; Mårtensson, N.; Puglia, C.; Brena, B.; Nyberg, M.; Luo, Y., The electronic structure of iron phthalocyanine probed by photoelectron and x-ray absorption spectroscopies and density functional theory calculations. *J. Chem. Phys.* **2006,** *125* (3), 034709.
84. Peisert, H.; Knupfer, M.; Fink, J., Electronic structure of partially fluorinated copper phthalocyanine (CuPCF4) and its interface to Au(100). *Surf. Sci.* **2002,** *515* (2-3), 491-498.
85. Adler, H.; Paszkiewicz, M.; Uihlein, J.; Polek, M.; Ovsyannikov, R.; Basova, T. V.; Chasse, T.; Peisert, H., Interface Properties of VOPc on Ni(111) and Graphene/Ni(111): Orientation-Dependent Charge Transfer. *J. Phys. Chem. C* **2015,** *119* (16), 8755-8762.
86. Ruocco, A.; Evangelista, F.; Attili, A.; Donzello, M. P.; Betti, M. G.; Giovanelli, L.; Gotter, R., Copper-phthalocyanine ultra thin films grown onto Al(1 0 0) surface investigated by synchrotron radiation. *Journal of Electron Spectroscopy and Related Phenomena* **2004,** *137-140*, 165-169.
87. Peisert, H.; Knupfer, M.; Schwieger, T.; Auerhammer, J. M.; Golden, M. S.; Fink, J., Full characterization of the interface between the organic semiconductor copper phthalocyanine and gold. *J. Appl. Phys.* **2002,** *91* (8), 4872-4878.
88. Gargiani, P.; Angelucci, M.; Mariani, C.; Betti, M. G., Metal-phthalocyanine chains on the Au(110) surface: Interaction states versus d-metal states occupancy. *Phys Rev B* **2010,** *81* (8).
89. Grobosch, M.; Aristov, V. Y.; Molodtsova, O. V.; Schmidt, C.; Doyle, B. P.; Nannarone, S.; Knupfer, M., Engineering of the Energy Level Alignment at Organic Semiconductor Interfaces by Intramolecular

Degrees of Freedom: Transition Metal Phthalocyanines. *J. Phys. Chem. C* **2009,** *113* (30), 13219-13222.
90. Brumboiu, I. E.; Prokopiou, G.; Kronik, L.; Brena, B., Valence electronic structure of cobalt phthalocyanine from an optimally tuned range-separated hybrid functional. *J. Chem. Phys.* **2017,** *147* (4), 11.
91. Brumboiu, I. E.; Haldar, S.; Lüder, J.; Eriksson, O.; Herper, H. C.; Brena, B.; Sanyal, B., Influence of Electron Correlation on the Electronic Structure and Magnetism of Transition-Metal Phthalocyanines. *Journal of Chemical Theory and Computation* **2016,** *12* (4), 1772-1785.
92. Ellis, T. S.; Park, K. T.; Ulrich, M. D.; Hulbert, S. L.; Rowe, J. E., Interaction of metallophthalocyanines (MPc,M=Co,Ni) on Au(001): Ultraviolet photoemission spectroscopy and low energy electron diffraction study. *Journal of Applied Physics* **2006,** *100* (9), 093515.
93. Ueno, N.; Kera, S.; Sakamoto, K.; Okudaira, K. K., Energy band and electron-vibration coupling in organic thin films: photoelectron spectroscopy as a powerful tool for studying the charge transport. *Applied Physics A* **2008,** *92* (3), 495-504.
94. Kera, S.; Yamane, H.; Ueno, N., First-principles measurements of charge mobility in organic semiconductors: Valence hole–vibration coupling in organic ultrathin films. *Progress in Surface Science* **2009,** *84* (5), 135-154.
95. Wang, J.; Wang, J.; Dougherty, D. B., Direct molecular quantification of electronic disorder in N, N'-Di-[(1-naphthyl)-N, N'-diphenyl]-1, 1'-biphenyl)-4, 4'-diamine on Au (111. *Journal of Vacuum Science & Technology B, Nanotechnology and Microelectronics: Materials, Processing, Measurement, and Phenomena* **2020,** *38* (5), 053401.
96. Koller, G.; Berkebile, S.; Oehzelt, M.; Puschnig, P.; Ambrosch-Draxl, C.; Netzer, F. P.; Ramsey, M. G., Intra- and intermolecular band dispersion in an organic crystal. *Science* **2007,** *317* (5836), 351-355.
97. Sättele, M. S.; Windischbacher, A.; Egger, L.; Haags, A.; Hurdax, P.; Kirschner, H.; Gottwald, A.; Richter, M.; Bocquet, F. C.; Soubatch, S.; Tautz, F. S.; Bettinger, H. F.; Peisert, H.; Chassé, T.; Ramsey, M. G.; Puschnig, P.; Koller, G., Going beyond Pentacene: Photoemission Tomography of a Heptacene Monolayer on Ag(110). *J. Phys. Chem. C* **2021,** *125* (5), 2918-2925.
98. Friedlein, R.; Crispin, X.; Simpson, C. D.; Watson, M. D.; Jackel, F.; Osikowicz, W.; Marciniak, S.; de Jong, M. P.; Samori, P.; Jonsson, S. K. M.; Fahlman, M.; Mullen, K.; Rabe, J. P.; Salaneck, W. R., Electronic structure of highly ordered films of self-assembled graphitic nanocolumns. *Phys Rev B* **2003,** *68* (19).
99. Ueno, N.; Kera, S., Electron spectroscopy of functional organic thin films: Deep insights into valence electronic structure in relation to charge transport property. *Progress in Surface Science* **2008,** *83* (10-12), 490-557.
100. Shang, M.-H.; Nagaosa, M.; Nagamatsu, S.-i.; Hosoumi, S.; Kera, S.; Fujikawa, T.; Ueno, N., Photoemission from valence bands of transition metal-phthalocyanines. *J. Electron Spectros. Relat. Phenomena* **2011,** *184* (3), 261-264.
101. Schönauer, K.; Weiss, S.; Feyer, V.; Lüftner, D.; Stadtmüller, B.; Schwarz, D.; Sueyoshi, T.; Kumpf, C.; Puschnig, P.; Ramsey, M. G.; Tautz, F. S.; Soubatch, S., Charge transfer and symmetry reduction at the CuPc/Ag(110) interface studied by photoemission tomography. *Phys. Rev. B: Condens. Matter* **2016,** *94* (20), 205144.
102. Lindner, S.; Treske, U.; Grobosch, M.; Knupfer, M., Charge transfer at F16CoPc and CoPc interfaces to Au. *Appl Phys a-Mater* **2011,** *105* (4), 921-925.
103. Lu, X.; Hipps, K. W.; Wang, X. D.; Mazur, U., Scanning Tunneling Microscopy of Metal Phthalocyanines: d7 and d9 Cases. *Journal of the American Chemical Society* **1996,** *118* (30), 7197-7202.
104. Lu, X.; Hipps, K. W., Scanning Tunneling Microscopy of Metal Phthalocyanines: d6 and d8 Cases. *The Journal of Physical Chemistry B* **1997,** *101* (27), 5391-5396.

105. Goiri, E.; Borghetti, P.; El-Sayed, A.; Ortega, J. E.; de Oteyza, D. G., Multi-Component Organic Layers on Metal Substrates. *Advanced Materials* **2016,** *28* (7), 1340-1368.
106. Bouju, X.; Mattioli, C.; Franc, G.; Pujol, A.; Gourdon, A., Bicomponent supramolecular architectures at the vacuum–solid interface. *Chem. Rev.* **2017,** *117* (3), 1407-1444.
107. El-Sayed, A.; Borghetti, P.; Goiri, E.; Rogero, C.; Floreano, L.; Lovat, G.; Mowbray, D. J.; Cabellos, J. L.; Wakayama, Y.; Rubio, A.; Ortega, J. E.; de Oteyza, D. G., Understanding Energy-Level Alignment in Donor-Acceptor/Metal Interfaces from Core-Level Shifts. *Acs Nano* **2013,** *7* (8), 6914-6920.
108. Wakayama, Y., On-surface molecular nanoarchitectonics: From self-assembly to directed assembly. *Jpn. J. Appl. Phys.* **2016,** *55* (11), 1102AA.
109. Henneke, C.; Felter, J.; Schwarz, D.; Stefan Tautz, F.; Kumpf, C., Controlling the growth of multiple ordered heteromolecular phases by utilizing intermolecular repulsion. *Nature Materials* **2017,** *16* (6), 628-633.

TOC Figure